Check for updates

View Article Online
View Journal

PCCP
Physical Chemistry Chemical Physics

Accepted Manuscript

This article can be cited before page numbers have been issued, to do this please use: N. Abdou, Q. Wu, L. Evenäs, A. Martinelli and A. Matic, *Phys. Chem. Chem. Phys.*, 2026, DOI: 10.1039/D6CP00353B.

This is an Accepted Manuscript, which has been through the Royal Society of Chemistry peer review process and has been accepted for publication.

Accepted Manuscripts are published online shortly after acceptance, before technical editing, formatting and proof reading. Using this free service, authors can make their results available to the community, in citable form, before we publish the edited article. We will replace this Accepted Manuscript with the edited and formatted Advance Article as soon as it is available.

You can find more information about Accepted Manuscripts in the Information for Authors.

Please note that technical editing may introduce minor changes to the text and/or graphics, which may alter content. The journal's standard Terms & Conditions and the Ethical guidelines still apply. In no event shall the Royal Society of Chemistry be held responsible for any errors or omissions in this Accepted Manuscript or any consequences arising from the use of any information it contains.

ROYAL SOCIETY OF CHEMISTRY

rsc.li/pccp

View Article Online
DOI: 10.1039/D6CP00353B

Journal Name

ARTICLE TYPE

Cite this: DOI: 00.0000/xxxxxxxxxx

Impact of Anion Mixing on Li^+ Coordination and Transport Properties in Pyrrolidinium-Based Ionic Liquid Electrolytes

Nicole Abdou,[a‡*] Quan Wu,[b‡] Lars Evenäs,[a] Anna Martinelli,[a] and Aleksandar Matic[b*]

Received Date
Accepted Date

DOI: 00.0000/xxxxxxxxxx

A series of pyrrolidinium-based ionic liquid electrolytes were investigated to explore the potential benefits of incorporating mixed anions, here bis(fluorosulfonyl)imide and bis(trifluoromethylsulfonyl)imide. The effect of mixing anions on fundamental physicochemical properties was investigated, with particular emphasis on transport properties and lithium-ion coordination. More specifically, the electrolytes were systematically characterized in terms of phase behavior, density, viscosity, transport properties (ionic conductivity and self-diffusion), and intermolecular interactions. The results show that mixing anions modifies the nature of intermolecular interactions, which in turn alters the coordination of the Li^+ to its counterions. In the case of $(LiFSI)_{0.2}(Pyr_{14}TFSI)_{0.8}$ sample, this resulted in improved thermal and transport properties, anticipating an improved performance in lithium-ion batteries.

1 Introduction

Ionic liquids (ILs) are a unique class of compounds that consist of (ideally) only ions and that have a melting point below 100 °C.[1] Notably, by selecting a specific combination of anions and cations, the physico-chemical properties of an ionic liquid can be tuned to suit a specific application.[2] Further, compared to conventional solvents, ILs exhibit broader electrochemical stability windows, good ionic conductivity along with high thermal stability, non-flammability and low volatility. Consequently, they have been extensively studied for various applications, such as catalysis,[3] gas separation,[4–6] and energy storage devices, including lithium-ion batteries.[7–9]

Among the vast variety of ionic liquids, those based on pyrrolidinium have been extensively studied for lithium-ion batteries due to their capacity to support lithium electrochemistry and promote the formation of a stable solid electrolyte interphase (SEI).[10,11] However, a key challenge in using ionic liquids in Li-ion batteries, is their limited transport properties (*i.e.*, slow Li^+ transport) and strong Li^+–anion interactions. Several strategies have been considered to address this issue, mainly aiming to enhance the diffusivity of the lithium ions. These include the use of molecular additives,[12] eutectic mixtures,[13,14] and binary/ternary ionic liquid systems.[15–19] Appetecchi *et al.* investigated a mixture of N-methyl-N-propyl pyrrolidinium bis(fluorosulfonyl)imide ($Pyr_{13}FSI$) and N-butyl-N-propyl pyrrolidinium bis(trifluoromethanesulfonyl)imide ($Pyr_{14}TFSI$) ILs with 0.3 M of either lithium hexafluorophosphate ($LiPF_6$) or lithium bis(trifluoromethanesulfonyl)imide (LiTFSI) salts. Their findings demonstrated enhanced ionic conductivity in ternary systems compared to binary ones, with a stronger effect at low temperatures.[20] Zhou *et al.* examined the phase behavior of the same systems, reporting the absence of phase transitions beyond 0.3 molar ratio with either salt.[21,22] Moreover, Bayley *et al.* studied ternary systems having Pyr_{13} as the common cation, paired with either FSI or TFSI anions over a broad compositional range in the presence of a lithium salt (0.5 m). Their results showed increased diffusivity of Li and TFSI ions upon addition of FSI.[23] Nádherná *et al.* investigated the electrochemical performance, in Li-ion batteries, of binary systems containing 0.7 m LiFSI or LiTFSI in $Pyr_{14}TFSI$. The authors reported higher charge/discharge capacities and improved electrochemical stability in the $LiFSI/Pyr_{14}TFSI$ mixed anion system.[24] Similarly, Lahiri *et al.* observed comparable results in a 1 M $LiTFSI/Pyr_{14}FSI$ system.[25]

To strengthen the understanding of the molecular interactions and transport mechanisms in these mixed-anion ionic liquid electrolytes, a multi-technique approach was employed to investigate mixtures of Pyr_{14}-based ionic liquids and lithium salts. An in-depth analysis of their phase behavior, transport properties, Li-ion coordination and intermolecular interactions was conducted, providing a side-by-side explanation of how Li^+ mobility relates to Li-ion coordination.

[a] *Department of Chemistry and Chemical Engineering, Chalmers University of Technology, SE-412 96 Gothenburg, Sweden. E-mail: nicole.abdou@chalmers.se*
[b] *Department of Physics, Chalmers University of Technology, SE-412 96 Gothenburg, Sweden. E-mail: matic@chalmers.se*
‡ These authors contributed equally to this work.
† Supplementary Information available: viscosity, density, ionic conductivity and self-diffusion coefficient values. See DOI: 00.0000/00000000.

Open Access Article. Published on 23 April 2026. Downloaded on 4/23/2026 10:39:49 PM.
This article is licensed under a Creative Commons Attribution 3.0 Unported Licence.

Physical Chemistry Chemical Physics Accepted Manuscript

View Article Online
DOI: 10.1039/D6CP00353B

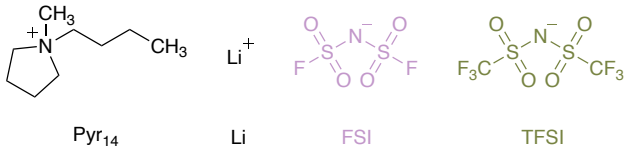

Fig. 1 Molecular structure of the 1-butyl-1-methylpyrrolidinium (Pyr_{14}) and lithium (Li) cations, and the bis(fluorosulfonyl)imide (FSI) and the bis(trifluoromethylsulfonyl)imide (TFSI) anions.

2 Experimental details

2.1 Chemicals

The lithium bis(trifluoromethylsulfonyl)imide (LiTFSI) (99.9 %) and lithium bis(fluorosulfonyl)imide (LiFSI) (99.9 %) salts, 1-butyl-1-methylpyrrolidinium bis(fluorosulfonyl)imide ($Pyr_{14}FSI$) (99.9 %) and 1-butyl-1-methylpyrrolidinium bis(trifluoromethylsulfonyl)imide ($Pyr_{14}TFSI$) (99.9 %) ionic liquids were purchased from Solvionic. The molecular structures of the ions found in the ionic liquids and in the salts are given in Figure 1. All compounds were dried under vacuum in a Büchi oven at 353 K for 12 hours, then stored in an argon-filled glovebox, before mixing and investigations.

2.2 Preparation

Samples were prepared by mixing ionic liquids and Li salts in a $0.2LiA_1{:}0.8Pyr_{14}A_2$ molar ratio, where A_1 and A_2 represent the FSI or the TFSI anion. All samples were prepared and stored in an argon-filled glovebox with O_2 and H_2O levels below 1 ppm. Throughout the following text the samples are named $(LiA_1)_{0.2}(Pyr_{14}A_2)_{0.8}$.

2.3 Methods

Differential Scanning Calorimetry (DSC). DSC measurements were performed using a DSC 250 from TA Instruments. Samples were placed in hermetic aluminum pans and sealed in an argon-filled glovebox. DSC thermograms were collected under helium flow (50 mL/min), over the temperature range 123 K to 373 K with heating and cooling rates of 5 K/min. Two scans were recorded for each measurement. The glass transition temperatures (T_g) were extracted from the second heating scan curves using sigmoid functions and identifying the inflection points.

Viscosity and density. Viscosity and density measurements were carried out using an Anton Paar DMA 4500 M oscillation U-tube densitometer over the temperature range 293 K to 353 K in 10 K increments. The density accuracy is about ± 0.0001 g/cm^3. The viscosity was determined using the Lovis 2000 ME rolling ball viscometer module, by which the dynamic viscosity (μ) was estimated from the density of the fluid (ρ) and the velocity of the falling ball (ν), as $\mu = \rho \cdot \nu$. The viscosity measurement has an accuracy of up to 0.1% and a repeatability of 0.5%. The temperature accuracy is ± 0.02 K with a repeatability of ± 0.005 K.

Dielectric Spectroscopy. Conductivity data were collected using a Novocontrol GmBH broadband dielectric spectrometer, parallel plate sample cell with stainless steel electrodes and a 3 mm spacer. Measurements were conducted in the frequency range 10^{-2} – 10^{7} Hz and the temperature range 173 K – 373 K. Data were collected every 10 K with a stabilization time of 180 s at each temperature. From three repeated measurements of the same solution, a value for the standard deviation has been estimated.

Nuclear Magnetic Resonance Diffusometry. NMR experiments were performed using an AVANCE III HD Bruker NMR spectrometer, operating at 14.1 T and equipped with a Diff30 probe connected to a 60 A gradient amplifier. RF coil inserts of a 5 mm 1H/2H double coil, a 5 mm 19F single coil, and a 5 mm 7Li single coil configuration were used. The self-diffusion coefficients of the different species, *i.e.*, Pyr_{14} (^{1}H), FSI/TFSI (^{19}F) and Li cation (^{7}Li) were determined at five different temperatures in the range 298 K – 353 K. A 5 mm NMR tube was filled ($\sim$ 1.5 cm) with the liquid sample and sealed in the glovebox using PTFE sealing tape. A regular stimulated echo NMR sequence (diffste) was used at room temperature. However, a double stimulated echo NMR sequence (diffDste) was employed at higher temperatures, to ensure that thermal convection did not affect the results. A 18 μs 90-degree pulse, 2 s acquisition time, 5 s recycling delay, 100 ms diffusion delay (Δ) and 1 ms gradient pulse duration (δ) were used. The maximum gradient strength (g) varied in the range 100 – 1200 Gauss/cm while keeping k constant, k is defined as:

$$k = (\delta \cdot \gamma \cdot g)^2(\Delta - \delta/3) \quad (1)$$

where Δ is the diffusion delay time, δ is the gradient pulse duration, γ is the gyromagnetic ratio of the studied nucleus and g is the gradient strength.

The gradient strengths were calibrated using reference samples with known self-diffusion coefficients; the ^{1}HDO trace signal in D_2O reference sample, hexafluorobenzene (C_6F_6) and a standard 1M LiCl in H_2O sample for ^{1}H, ^{19}F and ^{7}Li respectively.[26] To determine the intensity attenuation, the average of all ^{1}H NMR signals was considered for the Pyr_{14} cation. For the Li cation, the signal at -0.4 ppm in the ^{7}Li spectrum was utilized, while the signals at -80 ppm and 50 ppm in the ^{19}F spectrum, were used for the TFSI and FSI anions, respectively.

Raman Spectroscopy. Raman spectra were recorded using a Bruker MultiRAM Fourier transform Raman spectrometer equipped with a Nd:YAG laser (1064 nm) and a liquid nitrogen-cooled Ge diode detector. The nominal laser power was set to 720 mW, with a spectral resolution of 2 cm^{-1} (full width at half-maximum). A Blackman−Harris three-term window function was applied for apodization, and the spectra were acquired as the average of 1000 scans. In order to estimate the integrated areas under selected peaks, a multi-peak fitting procedure based on a linear background and Voigt profiles was applied using the Origin lab software. The spectral region 680–780 cm^{-1} was deconvoluted into six contributions, corresponding to spectroscopically free FSI (I, separated from cations), weakly coordinated FSI (II, contact ion pairs), strongly coordinated FSI–Li$^+$ (III, ion aggregates), the two conformers (*cisoid* (IV) and *transoid* (V)) of spectroscopically free TFSI and coordinated TFSI–Li$^+$ (VI). In the fitting procedure, peak positions, full widths at half maximum (FWHM), and Voigt profiles were fixed while heights were left as a free fit parameter. The population of the "free" and "coordi-

Open Access Article. Published on 23 April 2026. Downloaded on 4/23/2026 10:39:49 PM.
This article is licensed under a Creative Commons Attribution 3.0 Unported Licence.

Physical Chemistry Chemical Physics Accepted Manuscript

View Article Online
DOI: 10.1039/D6CP00353B

Open Access Article. Published on 23 April 2026. Downloaded on 4/23/2026 10:39:49 PM.
This article is licensed under a Creative Commons Attribution 3.0 Unported Licence.

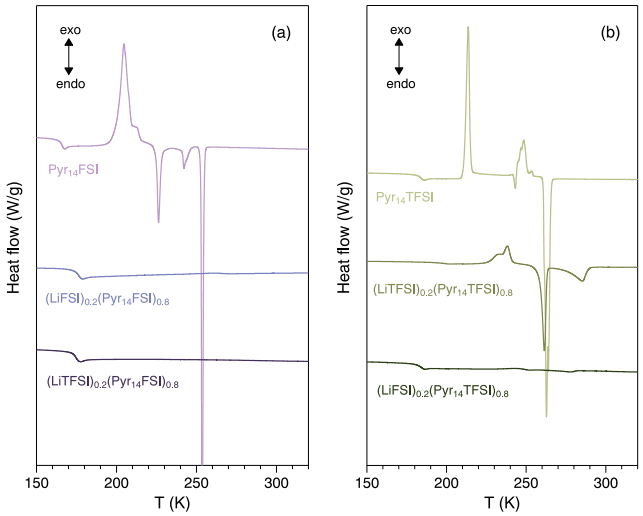

Fig. 2 DSC thermograms of $Pyr_{14}FSI$ (a) and $Pyr_{14}TFSI$ (b) based samples.

nated" anions were estimated from the relative intensities of the six components, as expressed below:

$$C_{\text{free FSI}} = \frac{A_{\text{I}}}{A_{\text{I}} + A_{\text{II}} + A_{\text{III}}} \quad (2)$$

$$C_{\text{coordinated FSI}} = \frac{A_{\text{II}} + A_{\text{III}}}{A_{\text{I}} + A_{\text{II}} + A_{\text{III}}} \quad (3)$$

$$C_{\text{free TFSI}} = \frac{A_{\text{IV}} + A_{\text{V}}}{A_{\text{IV}} + A_{\text{V}} + A_{\text{VI}}} \quad (4)$$

$$C_{\text{coordinated TFSI}} = \frac{A_{\text{VI}}}{A_{\text{IV}} + A_{\text{V}} + A_{\text{VI}}} \quad (5)$$

where A_{I}, A_{II}, A_{III}, A_{IV}, A_{V}, and A_{VI} are the integrated areas of the contributions I, II, III, IV, V and VI, respectively. These calculations are valid assuming that the Raman activities of the different TFSI and FSI conformations are equivalent,[27,28] so the integrated areas directly reflect their relative populations. Then, the average number of FSI and TFSI anions coordinating to Li^+ ($N_{\text{anion-Li}^+}$), was determined using:

$$N_{\text{anion-Li}^+} = \frac{C_{\text{coordinated anion}}}{x} \quad (6)$$

where x is the molar fraction of Li^+ ions.

3 Results and discussion

For a comprehensive understanding of the transport properties of the electrolytes at focus in this work, their phase behavior, viscosity, density, ionic conductivity and self-diffusion, as well as intermolecular interactions, with focus on coordination, were investigated.

3.1 Phase behavior

The phase behavior was investigated by DSC, Figure 2. Both neat ionic liquids, $Pyr_{14}FSI$ and $Pyr_{14}TFSI$, show melting peaks and glass transitions (T_g). The T_g of $Pyr_{14}FSI$ is found around 165 K, while that of $Pyr_{14}TFSI$ is slightly higher, observed at about 184 K.[29] In addition, the DSC curves of the neat ionic liquids reveal cold crystallization and solid–solid transitions. However, the phase behavior is significantly altered with the addition of Li salts. Either salt in the $Pyr_{14}FSI$-based systems, inhibits recrystallization and stabilizes the liquid phase down to the T_g, which is found at 175 K. For $Pyr_{14}TFSI$ with added LiTFSI, recrystallization and melting are still observed, however these transitions are suppressed upon mixing anions, *i.e.*, with the addition of LiFSI. Interestingly, the glass transition temperature increases by 11 K when LiTFSI is added to $Pyr_{14}TFSI$, whereas a T_g similar to that of the neat IL is observed for the mixed-anion system (LiFSI added to $Pyr_{14}TFSI$), see also values in Table 1. Thus, the incorporation of LiFSI into a TFSI-based ionic liquid has a more pronounced effect compared to the reversed scenario. Interestingly, an opposite trend was observed for imidazolium-based electrolytes.[30]

Table 1 Glass transition temperatures (T_g) of all ionic liquid electrolytes, extracted from the second heating scan of the DSC curve.

Sample	T_g (K)
$Pyr_{14}FSI$	165
$(LiFSI)_{0.2}(Pyr_{14}FSI)_{0.8}$	175
$(LiTFSI)_{0.2}(Pyr_{14}FSI)_{0.8}$	175
$Pyr_{14}TFSI$	184
$(LiTFSI)_{0.2}(Pyr_{14}TFSI)_{0.8}$	195
$(LiFSI)_{0.2}(Pyr_{14}TFSI)_{0.8}$	184

3.2 Viscosity and Density

Viscosity and density values measured as a function of temperature, are shown in Figure 3a-b. Corresponding values are summarized in Table S1. In $Pyr_{14}FSI$-based electrolytes, the addition of either lithium salt leads to an increase in both density and viscosity. For the electrolytes based on $Pyr_{14}TFSI$, the addition of LiTFSI salt leads to an increase in density and viscosity compared to the neat ionic liquid. Whereas, upon the addition of LiFSI, these increases are less pronounced, resulting in lower density and viscosity compared to the LiTFSI-containing electrolytes. Overall, $Pyr_{14}FSI$-based electrolytes exhibit lower viscosity and density compared to the $Pyr_{14}TFSI$-based electrolytes, as previously reported in the literature.[31] These results suggest that anion mixing in $Pyr_{14}TFSI$-based electrolytes significantly modifies the intermolecular interactions, with possible effects on the Li^+-anion coordination.

3.3 Transport properties

The ionic conductivity was measured in the temperature range 193 K – 373 K, using a broadband dielectric spectrometer (BDS), Figure 3c. The ionic conductivity values are summarized in Table S2. For all electrolytes, the ionic conductivity increases with increasing temperature. The neat $Pyr_{14}FSI$ exhibits higher ionic conductivity than $Pyr_{14}TFSI$, in agreement with the viscosity trend above and with the literature.[31] In general, the addition of a Li salt to the neat ionic liquids leads to a decrease in ionic conductivity, which can be attributed to the corresponding increase in viscosity discussed above.

The measured density, viscosity and conductivity data were used to create a Walden plot with the aim to highlight differ-

Physical Chemistry Chemical Physics Accepted Manuscript

View Article Online
DOI: 10.1039/D6CP00353B

Open Access Article. Published on 23 April 2026. Downloaded on 4/23/2026 10:39:49 PM.
This article is licensed under a Creative Commons Attribution 3.0 Unported Licence.

Physical Chemistry Chemical Physics Accepted Manuscript

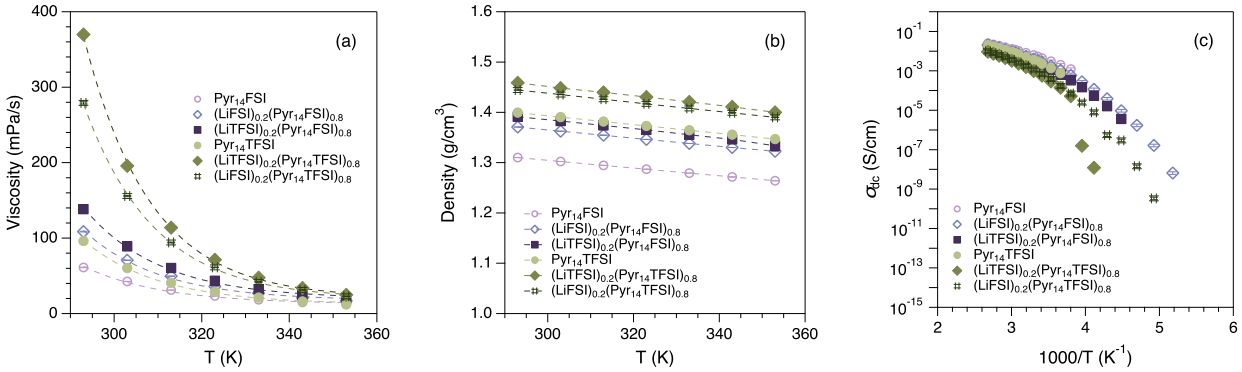

Fig. 3 Viscosity (a), density (b) and ionic conductivity (c) values measured as a function of temperature. The dashed lines are guides to the eyes. The error bars are smaller than the plotted symbols and are therefore not visible.

ences in ionic association and related transport mechanisms. The Walden plot is generally based on the Walden equation described by Angell *et al.*:[32]

$$\Lambda \cdot \eta^{\alpha} = C \tag{7}$$

where Λ is the molar conductivity, η is the viscosity, α is an adjustable parameter and C is a temperature dependent constant.

The Walden plots of all electrolytes are shown in Figure 4. In this plot, the diagonal line represents the behavior expected from an aqueous solution of 0.01 M KCl, in which all ions are assumed to be dissociated and to diffuse independently of each other. A negative deviation from the reference line, also known as the ideal line, can be seen as a measure of ion association within the ionic liquid system, a rationale for the conductivity being lower than expected from the mobility of ions.[32] The data of all investigated ionic liquids fall below the ideal line, with deviations ranging from -0.140 to -0.343, increasing from the neat ionic liquids to the electrolytes (Table S3). This implies, according to Angell *et al.*, the presence of ionic interactions that prevent full ion dissociation.[32] Additionally, upon the addition of a salt, the Walden plots of the Pyr$_{14}$TFSI-based ionic liquids show a slightly greater deviation from the ideal line than those of Pyr$_{14}$FSI-based ionic liquids. The slopes of all plots, reflecting the temperature dependence of ion association, are approximately 0.90, consistent with values typically reported for ionic liquids.[32–35]

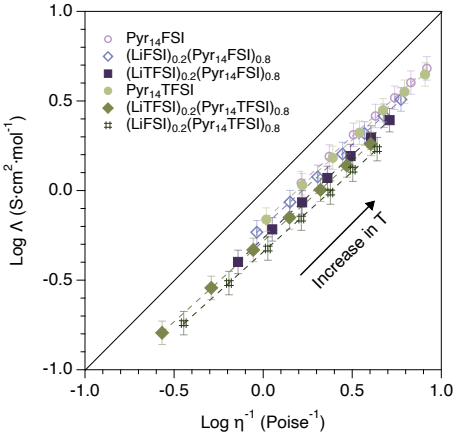

Fig. 4 Walden plot for Pyr$_{14}$FSI and Pyr$_{14}$TFSI based samples.

The ionic conductivity values of the mixed-anion electrolytes were also plotted on a T_g-scaled Arrhenius plot (an Angell's plot), normalizing the temperature scale to each material's glass transition temperature, Figure 5. The T_g values used in this approach are those obtained from the DSC data discussed above, also reported in Figure 1. This representation allows extending the discussion of ionic conductivity to the concept of fragility; fragility being a fundamental property of glass-forming liquids that describes how rapidly the dynamics change upon heating from the glass transition temperature T_g, or vice versa. In an Angell's plot, fragile liquids display a strong curvature whereas stronger liquids exhibit a closer to linear behavior. In Figure 5, the ionic conductivity values for the two samples converge onto a single curve, revealing similar fragility and indicating that their temperature-dependent conductivities evolve in a comparable manner relative to T_g, despite differences in composition and glass transition temperatures. Consequently, their dynamics change at a similar rate near T_g, where rapid changes in dynamics facilitate higher mobilities at elevated temperatures, an advantageous behavior for practical applications.[36]

To selectively distinguish Li^+ ion transport, which cannot be resolved by BDS, the self-diffusion coefficients of all involved ionic species, *i.e.*, Pyr$_{14}$, Li^+, FSI and TFSI, were estimated using NMR diffusometry, Figure 6a-f. The extracted self-diffusion coefficient values are summarized in Table S4. While for Pyr$_{14}$FSI, the anion exhibits higher diffusivity than the cation, the opposite trend is observed for Pyr$_{14}$TFSI. This finding aligns with earlier studies and may be attributed to the size difference between the FSI and TFSI anions.[37–40] When salts are added, the self-diffusion coefficients of all ions decrease due to increased viscosity, in agreement with the viscosity and conductivity data discussed above. Interestingly, the addition of LiFSI to Pyr$_{14}$TFSI leads to a smaller decrease in diffusion coefficient than the addition of LiTFSI (especially at lower temperatures). This difference may be attributed to the smaller size of the FSI anion, favoring fluidity. Importantly, in FSI-based systems, the self-diffusion coefficients of all ions, including the Li^+, remain higher than those in TFSI-based systems, consistent with previously reported results.[15,39] The relative contribution of Li^+ ions to the overall conductivity can be estimated by calculating the apparent transference number (t_{Li^+}) from the

View Article Online
DOI: 10.1039/D6CP00353B

Open Access Article. Published on 23 April 2026. Downloaded on 4/23/2026 10:39:49 PM.
This article is licensed under a Creative Commons Attribution 3.0 Unported Licence.

Physical Chemistry Chemical Physics Accepted Manuscript

diffusion data. High Li^+ transference numbers are essential for efficient charge–discharge performance in Li-ion batteries. Across all studied electrolytes, t_{Li^+} remains approximately 0.07 with negligible temperature dependence (Table S5). These values are consistent with the literature and indicate that the Li^+ contribution to the conductivity remains similar across all four electrolytes.

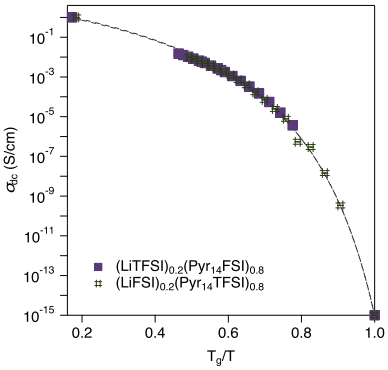

Fig. 5 T_g-scaled plot (Angell plot) of the ionic conductivity of $(LiTFSI)_{0.2}(Pyr_{14}FSI)_{0.8}$ and $(LiFSI)_{0.2}(Pyr_{14}TFSI)_{0.8}$. The dashed lines are guides to the eyes. The error bars are smaller than the plotted symbols and are therefore not visible.

To gain deeper insight into the degree of ion dissociation, the ratio of molar conductivity Λ/Λ_{NE}, also known as ionicity, was estimated.[41–43] Λ is the molar conductivity obtained from impedance measurements (eq. 8), while Λ_{NE} is the molar conductivity calculated from the self-diffusion coefficients using the Nernst-Einstein equation (eq. 9):

$$\Lambda = \frac{\sigma_{dc} \cdot M_{sol}}{\rho} \tag{8}$$

with σ_{dc} being the ionic conductivity measured by BDS, M_{sol} the molar mass of the solution $= \chi_{IL} \cdot M_{IL} + \chi_{salt} \cdot M_{salt}$ and ρ the density of the solution.

$$\Lambda_{NE} = \frac{(x_{Pyr_{14}} \cdot D_{Pyr_{14}} + x_{TFSI} \cdot D_{TFSI} + x_{FSI} \cdot D_{FSI} + x_{Li^+} \cdot D_{Li^+}) \cdot F^2}{R \cdot T} \tag{9}$$

where F is the Faraday constant, R is the universal gas constant and x_i is the molar ratio of the i^{th} component. The molar conductivities and ionicity values are summarized in Table S6. Figures 7a and 7b show that Λ is smaller than Λ_{NE} in all systems and at all temperatures. Consequently, the ionicity Λ/Λ_{NE} shows a value ≤ 1 in all studied liquids, as shown in Figure 7c, indicating that some ionic species diffuse in pairs or clusters hence not contributing to the macroscopically measured ionic conductivity, in line with the trend observed in the Walden plot (Figure 4). The ionicity decreases in both systems with the addition of Li salt, in particular when anions are mixed, highlighting overall stronger interactions and aggregate formation in the electrolytes.

3.4 Ion coordination

Further insight into the nature of intermolecular interactions can be obtained by Raman spectroscopy. Room temperature Raman spectra were recorded for both the neat ionic liquids and the electrolytes, Figure 8. In $Pyr_{14}TFSI$-based systems, the strongest vibrational mode occurs around 743 cm^{-1}, corresponding to the expansion-contraction mode of the TFSI anion (ν_s S-N-S and ν_s CF_3).[44] The sensitivity of this mode to the coordination of the anion has been thoroughly investigated using both experimental and theoretical methods.[27,45] In the neat $Pyr_{14}TFSI$, TFSI exhibits two coexisting, weakly coordinated conformers (*cis* and *trans*). The two conformers give rise to two closely spaced bands in the Raman spectrum between 740 and 744 cm^{-1}. With the addition of LiTFSI, a new Raman band appears at higher frequencies, around 748 cm^{-1}, attributed to TFSI anions coordinating to the Li^+ cation.[46–48] The average number of TFSI anions around a Li^+ was calculated to be 2.17 (Table 2).[48] Similarly, FSI in $Pyr_{14}FSI$ exhibit two conformations (C_1 and C_2) that coexist at room temperature, associated to two (theoretically calculated) closely spaced Raman modes at 725 and 732 cm^{-1}. However, a single broader Raman band is typically observed experimentally around 730 cm^{-1}. Upon addition of LiFSI, an additional Raman mode has been reported in the literature at approximately 744 cm^{-1}, corresponding to FSI coordinated to Li^+.[49,50] The calculated average number of FSI surrounding Li^+ is 3.33 (Table 2), which is higher than the corresponding number of TFSI in the $(LiTFSI)_{0.2}(Pyr_{14}TFSI)_{0.8}$ sample (2.17). This suggests that Li^+ coordination involves more FSI than TFSI anions, consistent with the results discussed above.

Table 2 Average number of Li^+-coordinated FSI and TFSI anions ($N_{anion\text{-}Li^+}$) estimated from peak fitting the Raman spectra.

Samples	$N_{FSI\text{-}Li^+}$	$N_{TFSI\text{-}Li^+}$
$(LiTFSI)_{0.2}(Pyr_{14}TFSI)_{0.8}$	–	2.17
$(LiFSI)_{0.2}(Pyr_{14}FSI)_{0.8}$	3.33	–
$(LiFSI)_{0.2}(Pyr_{14}TFSI)_{0.8}$	0.73	1.78
$(LiTFSI)_{0.2}(Pyr_{14}FSI)_{0.8}$	2.70	0.54

However, mixing anions results in a more complex Li^+ solvation structure. Six Raman modes were identified and fitted, corresponding to two conformers of weakly coordinated TFSI, one Li^+–coordinated TFSI, one free FSI, one weakly coordinated FSI (contact ion pairs) and one strongly FSI coordinated – Li^+ (ion aggregates). The calculated average numbers of FSI and TFSI anions coordinating Li^+ are 0.73 and 1.78, for $(LiFSI)_{0.2}(Pyr_{14}TFSI)_{0.8}$ sample, and 2.70 and 0.54 for $(LiTFSI)_{0.2}(Pyr_{14}FSI)_{0.8}$ sample. Consequently, the average number of anions around each Li^+ in $(LiFSI)_{0.2}(Pyr_{14}TFSI)_{0.8}$ sample, with mixed anions, is 2.51 slightly higher than in the single-anion electrolyte $(LiTFSI)_{0.2}(Pyr_{14}TFSI)_{0.8}$ (2.17). This can be explained by the higher ability of FSI to coordinate Li^+. In contrast, the average number of anions around Li^+ remains nearly unchanged in the $Pyr_{14}FSI$-based samples.

The total number of anions coordinated to Li ions in the IL system plays a significant role in determining the strength of the Li-ion solvation structure, which in turn influences the transport properties of the Li ion. We find that the order of this coordination across the four samples is as follows: $(LiTFSI)_{0.2}(Pyr_{14}TFSI)_{0.8} < (LiFSI)_{0.2}(Pyr_{14}TFSI)_{0.8} < (LiTFSI)_{0.2}(Pyr_{14}FSI)_{0.8} \leq (LiFSI)_{0.2}(Pyr_{14}FSI)_{0.8}$.

These results are consistent with the higher Li^+ self-diffusion

View Article Online
DOI: 10.1039/D6CP00353B

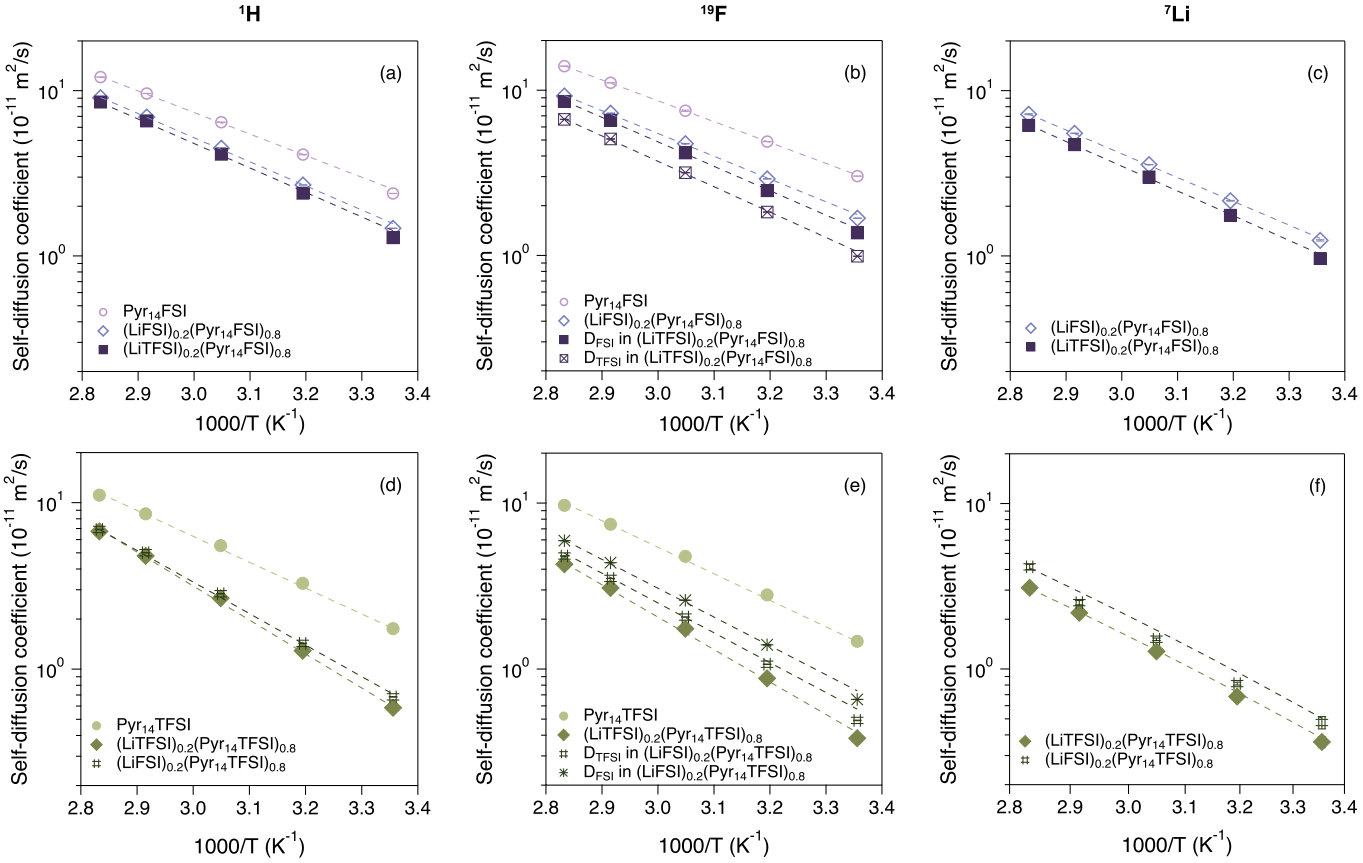

Fig. 6 The three upper panels and the three bottom panels show the self-diffusion coefficients estimated for the $Pyr_{14}FSI$ based (a–c) and the $Pyr_{14}TFSI$ based (d–f) samples, respectively. The first (a and d), second (b and e) and third (c and f) columns show self-diffusion values measured from the ^{1}H, ^{19}F and ^{7}Li nuclei. Dashed lines are guides to the eyes. The error bars are smaller than the plotted symbols and are therefore not visible.

coefficients observed for $Pyr_{14}FSI$-based systems compared to their counterparts. Figure 9 illustrates the correlation between the average number of Li-coordinated anions ($N_{anion\text{-}Li^+}$) and Li^+ mobility (D_{Li^+}), showing that an increase in $N_{anion\text{-}Li^+}$ is associated with an increase in D_{Li^+}.

Conclusions

In summary, mixtures of pyrrolidinium-based ionic liquids and 0.2 mole fraction of lithium salts with either identical or mixed anions were investigated with a focus on their physicochemical properties, particularly Li-ion diffusion and coordination. The incorporation of lithium salt generally leads to increased viscosity, higher glass transition temperature (T_g), reduced ionic conductivity and slower ion diffusivity compared to neat ionic liquid systems. Notably, mixing anions shows a more pronounced effect in $Pyr_{14}TFSI$-based systems, where the addition of FSI anions significantly lowers T_g and enhances both conductivity and ion diffusivity. This behavior is likely due to the smaller size and greater Li-coordinating ability of the FSI anion compared to TFSI, which alters the intermolecular interactions within the system. Despite the positive impact of the mixed-anion approach, the larger size of the TFSI anion has a dominant impact reducing ion transport and increasing viscosity, relative to the systems rich in FSI. Although some observed effects, such as the increased viscosity and decreased conductivity, may be expected to persist at other Li salt concentrations, as reported in the literature, further studies are necessary to confirm these trends in the herein studied systems.[30,35] Among the mixed-anion solutions investigated in this work, $(LiTFSI)_{0.2}(Pyr_{14}FSI)_{0.8}$ emerges as a promising candidate as a lithium-ion battery electrolyte, due to its favorable balance of transport properties and thermal behavior.

Author contributions

Nicole Abdou: Data curation, Formal analysis, Investigation, Methodology, Visualization, Writing - original draft, Writing - review & editing. Quan Wu: Data curation, Formal analysis, Investigation, Methodology, Writing - review & editing. Lars Evenäs: Investigation, Validation, Writing - review & editing. Anna Martinelli: Funding acquisition, Supervision, Validation, Writing - review & editing. Aleksandar Matic: Conceptualization, Funding acquisition, Resources, Supervision, Validation, Writing - review & editing.

Conflicts of interest

There are no conflicts to declare.

Data availability

Data will be made available on request.

Open Access Article. Published on 23 April 2026. Downloaded on 4/23/2026 10:39:49 PM.
This article is licensed under a Creative Commons Attribution 3.0 Unported Licence.

Physical Chemistry Chemical Physics Accepted Manuscript

View Article Online
DOI: 10.1039/D6CP00353B

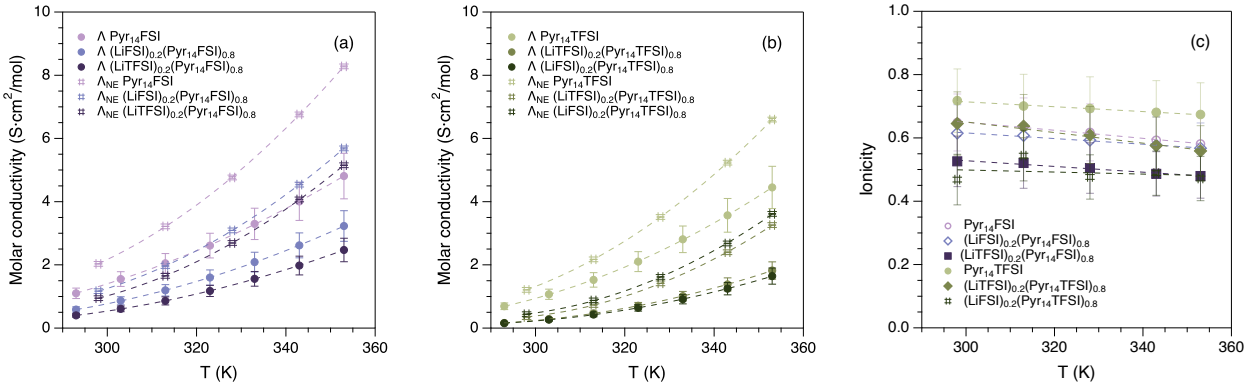

Fig. 7 Molar conductivities obtained from NMR and impedance measurements for $Pyr_{14}FSI$ (a) and $Pyr_{14}TFSI$ (b) based samples. Estimated ionicity values as a function of temperature (c).

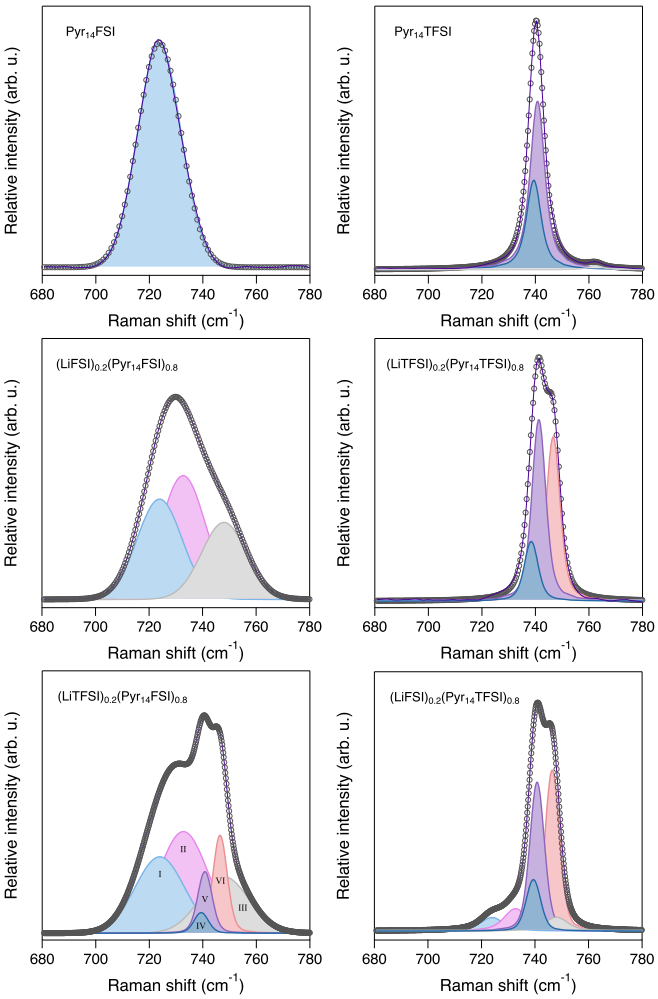

Fig. 8 Experimentally recorded Raman spectra (symbols), fitting peaks (colored Voigt profiles) and fit results (black lines) for all Pyr_{14}-based solutions. Peaks are labeled consistently across all six panels as follow: spectroscopically free FSI (I), weakly coordinated FSI (II), strongly coordinated FSI-Li^+ (III), *cis* (IV) and *trans* (V) conformers of spectroscopically free TFSI, and Li^+-coordinated TFSI (VI).

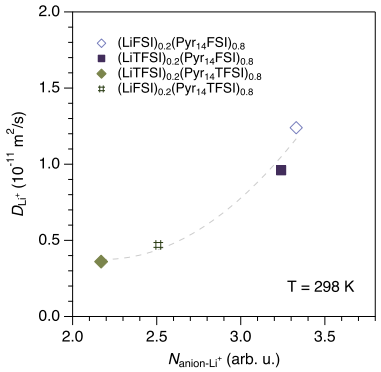

Fig. 9 The Li^+ self-diffusion coefficient (D_{Li^+}) as a function of the average number of Li^+-coordinated anions $N_{anion\text{-}Li^+}$). The dashed line is a guide to the eyes.

Acknowledgements

Nicole Abdou and Anna Martinelli kindly thank the Areas of Advance *Materials Science* and *Energy* at Chalmers University of Technology for the financial support. Quan Wu and Aleksandar Matic acknowledge the Swedish Electricity Storage and Balancing Centre (SESBC). This project is financed through the Swedish Electricity Storage and Balancing Centre (SESBC). The Centre is funded by the Swedish Energy Agency together with five academic and twenty-eight non-academic partners. The authors also thank the Swedish NMR Centre in Gothenburg for the allocated NMR time.

Notes and references

1 Z. Lei, B. Chen, Y.-M. Koo and D. R. MacFarlane, *Chemical Reviews*, 2017, **117**, 6633–6635.
2 M. Freemantle, *Chemical & Engineering News Archive*, 1998, **76**, 32–37.
3 M. Vafaeezadeh and H. Alinezhad, *Journal of Molecular Liquids*, 2016, **218**, 95–105.
4 Z. Dai, R. D. Noble, D. L. Gin, X. Zhang and L. Deng, *Journal of Membrane Science*, 2016, **497**, 1–20.
5 L. C. Tomé and I. M. Marrucho, *Chem. Soc. Rev.*, 2016, **45**, 2785–2824.
6 I. Harmanli, N. V. Tarakina, M. Antonietti and M. Oschatz, *Journal of the American Chemical Society*, 2021, **143**, 9377–9384.

Open Access Article. Published on 23 April 2026. Downloaded on 4/23/2026 10:39:49 PM.
This article is licensed under a Creative Commons Attribution 3.0 Unported Licence.

Physical Chemistry Chemical Physics Accepted Manuscript

View Article Online
DOI: 10.1039/D6CP00353B

Open Access Article. Published on 23 April 2026. Downloaded on 4/23/2026 10:39:49 PM.
This article is licensed under a Creative Commons Attribution 3.0 Unported Licence.

7 D. R. MacFarlane, N. Tachikawa, M. Forsyth, J. M. Pringle, P. C. Howlett, G. D. Elliott, J. H. Davis, M. Watanabe, P. Simon and C. A. Angell, *Energy Environ. Sci.*, 2014, **7**, 232–250.
8 M. WATANABE, *Electrochemistry*, 2016, **84**, 642–653.
9 M. Watanabe, M. L. Thomas, S. Zhang, K. Ueno, T. Yasuda and K. Dokko, *Chemical reviews*, 2017, **117**, 7190–7239.
10 M. Kerner and P. Johansson, *Batteries*, 2018, **4**, 10–22.
11 L. M. McGrath and J. F. Rohan, *Molecules*, 2020, **25**, 6002–6035.
12 F. Lundin, A. Idström, P. Falus, L. Evenäs, S. Xiong and A. Matic, *The Journal of Physical Chemistry C*, 2022, **126**, 16262–16271.
13 P. M. Bayley, A. S. Best, D. R. MacFarlane and M. Forsyth, *Phys Chem Chem Phys*, 2011, **13**, 4632–40.
14 M. Middendorf and M. Schonhoff, *J Phys Chem B*, 2024, **128**, 2939–2947.
15 F. Castiglione, G. Raos, G. B. Appetecchi, M. Montanino, S. Passerini, M. Moreno, A. Famulari and A. Mele, *Phys Chem Chem Phys*, 2010, **12**, 1784–92.
16 G. Annat, M. Forsyth and D. R. MacFarlane, *J Phys Chem B*, 2012, **116**, 8251–8258.
17 M. T. Clough, C. R. Crick, J. Grasvik, P. A. Hunt, H. Niedermeyer, T. Welton and O. P. Whitaker, *Chem Sci*, 2015, **6**, 1101–1114.
18 M. Kunze, S. Jeong, G. B. Appetecchi, M. Schönhoff, M. Winter and S. Passerini, *Electrochimica Acta*, 2012, **82**, 69–74.
19 N. Abdou, A. Pipertzis, J. Swenson and A. Martinelli, *Journal of Molecular Liquids*, 2025, **437**, 128418–128427.
20 G. B. Appetecchi, M. Montanino, A. Balducci, S. F. Lux, M. Winterb and S. Passerini, *Journal of Power Sources*, 2009, **192**, 599–605.
21 Q. Zhou, W. A. Henderson, G. B. Appetecchi and S. Passerini, *The Journal of Physical Chemistry C*, 2010, **114**, 6201–6204.
22 Q. Zhou, P. D. Boyle, L. Malpezzi, A. Mele, J.-H. Shin, S. Passerini and W. A. Henderson, *Chemistry of Materials*, 2011, **23**, 4331–4337.
23 P. M. Bayley, A. S. Best, D. R. MacFarlane and M. Forsyth, *Chemphyschem*, 2011, **12**, 823–827.
24 M. Nádherná, J. Reiter, J. Moškon and R. Dominko, *Journal of Power Sources*, 2011, **196**, 7700–7706.
25 A. Lahiri, T. J. Schubert, B. Iliev and F. Endres, *Phys Chem Chem Phys*, 2015, **17**, 11161–11164.
26 M. Holz and H. Weingartner, *Journal of Magnetic Resonance (1969)*, 1991, **92**, 115–125.
27 M. Herstedt, M. Smirnov, P. Johansson, M. Chami, J. Grondin, L. Servant and J. C. Lassègues, *Journal of Raman Spectroscopy*, 2005, **36**, 762–770.
28 L. Li, S. Zhou, H. Han, H. Li, J. Nie, M. Armand, Z. Zhou and X. Huang, *Journal of The Electrochemical Society*, 2011, **158**, A74–A82.
29 M. Kunze, S. Jeong, E. Paillard, M. Winter and S. Passerini, *The Journal of Physical Chemistry C*, 2010, **114**, 12364–12369.
30 M. Kerner, N. Plylahan, J. Scheers and P. Johansson, *Phys Chem Chem Phys*, 2015, **17**, 19569–19581.
31 P. Gerlach, R. Burges, A. Lex-Balducci, U. S. Schubert and A. Balducci, *Journal of The Electrochemical Society*, 2020, **167**, 120546.
32 C. A. Angell, N. Byrne and J.-P. Belieres, *Accounts of Chemical Research*, 2007, **40**, 1228–1236.
33 W. Xu, E. I. Cooper and C. A. Angell, *The Journal of Physical Chemistry B*, 2003, **107**, 6170–6178.
34 K. Ueno, H. Tokuda and M. Watanabe, *Phys. Chem. Chem. Phys.*, 2010, **12**, 1649–1658.
35 H. Yoon, A. S. Best, M. Forsyth, D. R. MacFarlane and P. C. Howlett, *Phys. Chem. Chem. Phys.*, 2015, **17**, 4656–4663.
36 P. Sippel, P. Lunkenheimer, S. Krohns, E. Thoms and A. Loidl, *Scientific Reports*, 2015, **5**, 13922–13929.
37 J. B. Haskins, W. R. Bennett, J. J. Wu, D. M. Hernández, O. Borodin, J. D. Monk, C. W. J. Bauschlicher and J. W. Lawson, *The Journal of Physical Chemistry B*, 2014, **118**, 11295–11309.
38 F. Castiglione, E. Ragg, A. Mele, G. B. Appetecchi, M. Montanino and S. Passerini, *The Journal of Physical Chemistry Letters*, 2011, **2**, 153–157.
39 F. Lundin, A. Idström, P. Falus, L. Evenäs, S. Xiong and A. Matic, *The Journal of Physical Chemistry C*, 2022, **126**, 16262–16271.
40 F. Castiglione, M. Moreno, G. Raos, A. Famulari, A. Mele, G. B. Appetecchi and S. Passerini, *The Journal of Physical Chemistry B*, 2009, **113**, 10750–10759.
41 M. Gouverneur, J. Kopp, L. van Wullen and M. Schonhoff, *Phys Chem Chem Phys*, 2015, **17**, 30680–30686.
42 O. Holloczki, F. Malberg, T. Welton and B. Kirchner, *Phys Chem Chem Phys*, 2014, **16**, 16880–16890.
43 K. Ueno, H. Tokuda and M. Watanabe, *Phys Chem Chem Phys*, 2010, **12**, 1649–1658.
44 I. Rey, P. Johansson, J. Lindgren, J. C. Lassègues, J. Grondin and L. Servant, *The Journal of Physical Chemistry A*, 1998, **102**, 3249–3258.
45 J. C. Lassègues, J. Grondin, R. Holomb and P. Johansson, *Journal of Raman Spectroscopy*, 2007, **38**, 551–558.
46 S. Duluard, J. Grondin, J.-L. Bruneel, I. Pianet, A. Grélard, G. Campet, M.-H. Delville and J.-C. Lassègues, *Journal of Raman Spectroscopy*, 2008, **39**, 627–632.
47 J.-C. Lassègues, J. Grondin, C. Aupetit and P. Johansson, *The Journal of Physical Chemistry A*, 2009, **113**, 305–314.
48 J. Pitawala, A. Martinelli, P. Johansson, P. Jacobsson and A. Matic, *Journal of Non-Crystalline Solids*, 2015, **407**, 318–323.
49 K. Fujii, S. Seki, S. Fukuda, R. Kanzaki, T. Takamuku, Y. Umebayashi and S.-i. Ishiguro, *The Journal of Physical Chemistry B*, 2007, **111**, 12829–12833.
50 K. Fujii, H. Hamano, H. Doi, X. Song, S. Tsuzuki, K. Hayamizu, S. Seki, Y. Kameda, K. Dokko, M. Watanabe and Y. Umebayashi, *The Journal of Physical Chemistry C*, 2013, **117**, 19314–19324.

Physical Chemistry Chemical Physics Accepted Manuscript

Chalmers University of Technology
SE- 412 96 Gothenburg, Sweden
Nicole.abdou@chalmers.se
www.chalmers.se

View Article Online
DOI: 10.1039/D6CP00353B

Subject: Data Availability Statement

Dear Editor,

The numerical data used in this manuscript, *i.e.,* density, viscosity, ionic conductivity and self-diffusion coefficient values, are all reported in the Supporting Information.

Yours Sincerely,

Gothenburg on the 30th of January 2026
Dr. Nicole Abdou and co-workers

Nicole

Open Access Article. Published on 23 April 2026. Downloaded on 4/23/2026 10:39:49 PM.
This article is licensed under a Creative Commons Attribution 3.0 Unported Licence.

Physical Chemistry Chemical Physics Accepted Manuscript